Evaporation from Falling Saline Water Films in Laminar Transitional Flow

WALTER UNTERBERG and D. K. EDWARDS

University of California, Los Angeles, California

An analytical and experimental study was made of the evaporation from pure and saline water films flowing down a heated vertical surface at Reynolds numbers between 160 and 600. Visual observation showed free surface evaporation. Film continuity was poor for pure water, but good for saline water, because of the influence of temperature and salinity on surface tension gradients. Evaporation rates were predicted by (1) a constant-property boundary-layer type of laminar analysis; (2) the constant-property Dukler "eddy" treatment; and (3) a variable property laminar analysis that took into account the boiling point elevation due to salinity. The experimental evaporation rates could be correlated by dimensionless moduli arising out of the laminar analyses, but best quantitative agreement was found with the Dukler eddy treatment.

In typical falling film saline water evaporators, the condensation of steam on one side of a vertical wall produces evaporation of water vapor from a thin film of saline water flowing down the other side. This paper describes an analytical and experimental study of falling saline water film evaporation.

Isothermal nonevaporating liquid film flow under gravity down a vertical surface has been frequently investigated (*6, 25, 32*). Four regimes may be distinguished by film Reynolds number (*12*): true laminar (0 to 4-27), pseudo laminar (4-27 to 80-350), transitional (80-350 to 1,600-2,000) and turbulent (above 1,600-2,000). A laminar analysis by Nusselt (*23*) gave the film thickness as

$$h_{lam} = 0.909 \left(\frac{\nu^2}{g}\right)^{1/3} N_{Re}^{1/3}; N_{Re} = 4\,m/\mu$$

More sophisticated treatments (*16, 30*) have agreed with this result. In the other regimes there is eddy transport present within the falling film (*1, 10*). Dukler (*10*) used the Deissler (*9*) expressions for eddy viscosity to derive falling film thickness and heat transfer up to a Reynolds number of 50,000. His thickness coincides with the Nusselt value up to a Reynolds number of about 300 and at higher Reynolds numbers lies above it, in good agreement with experimental measurements (*11*). His local heat transfer coefficients vary with Reynolds number and Prandtl number and exceed laminar values (k/h_{lam}) throughout.

A falling liquid film is retained on a vertical surface by the action of surface tension. In heat and mass transfer applications it is extremely important to maintain a fully wetted surface, that is, a continuous film, for optimum performance. In such "free surface" evaporation, the latent heat is conducted from the hot surface across the liquid film to the free surface. With a ripply or wavy surface, local variations in surface temperature and salinity are created. These give rise to associated variations in surface tension which tend to cause surface movements. Depending on the variation of surface tension with temperature and salinity and on the mechanism and direction of the heat or mass transfer, the surface tension gradients may or may not tend to maintain a continuous liquid film at a given flow rate (*2, 3, 14, 21, 22*).

Effect of salinity on surface tension and the other thermophysical properties of saline water are shown in Figure 1. The Soret effect (*7*) is small, and the Dufour effect (*8*) has not been observed. The primary property variation is the boiling point elevation (B.P.E.) which reduces the net temperature difference across the liquid film. Further, after the saturation salinity is reached, solid salt precipitates out and interferes with equipment performance.

Survey of Experimental Literature

Falling film evaporation experiments cover a wide spectrum in variables, no two investigations having been carried out at comparable conditions (*2, 4, 5, 17* to *19, 22, 26, 27*). Film thicknesses during evaporation are not reported, and the evaporation surface was not observable in most cases to determine the evaporation mechanism, except for two (*17, 26*) with boiling and/or turbulent feed. Indications are that apparently conflicting experimental results may be explained by knowledge about: (1) the feed liquid characteristics, (2)

Walter Unterberg is also with Rocketdyne, a Division of North American Aviation, Inc., Canoga Park, California.

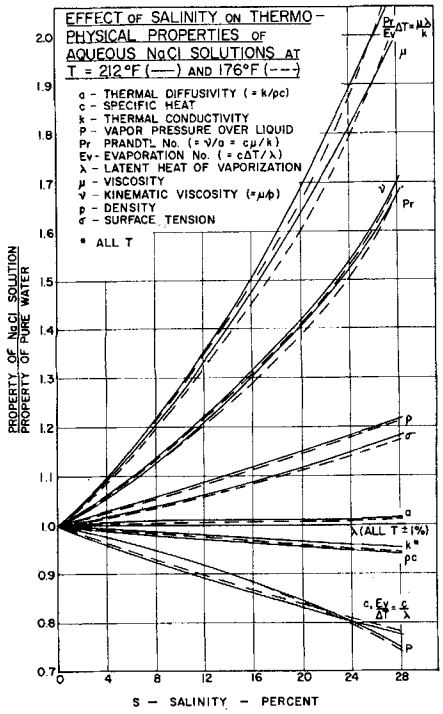

Fig. 1. Effect of salinity on thermophysical properties of aqueous sodium chloride solutions at T = 212°F. (-) and 176°F. (- - -).

the evaporation mechanism, and (3) the extent of wetting of the heating surface. If the feed consists of liquid at temperatures below the boiling point, a smooth film usually results, with free surface evaporation. If the feed is boiling and the temperature difference is high enough, evaporation takes place via nucleate boiling. In either case the extent of surface wetting is influenced by the combined action of gravity, viscous, and surface forces. These forces are functions of feed flow rate, salinity, and temperature, and of the evaporation temperature difference.

Two of the investigations compare experimental results with analytical models. Linke (*19*) performed a laminar film evaporation analysis, but found experimental ammonia evaporation rates to be higher than those predicted. Sinek and Young (*27*) used the Dukler (*10*) eddy treatment and allowed for boiling point elevation due to salinity and vapor bubbles in the boiling feed. They found agreement within 20% for data in the turbulent regime.

The present experimental investigation focuses on pseudo laminar and transitional film flow regimes (N_{Re} between 100 and 1,000) with controlled liquid feed, and provides for observation of the evaporation mechanism and the extent of surface wetting.

FALLING FILM EVAPORATION THEORY

Constant-Property Laminar Model

Since practical film thicknesses are of the order of 10^{-2} in., the two-dimensional incompressible laminar boundary-layer equations are applicable to express the velocity, temperature, and salinity variations in the liquid film. Salt is assumed to be transported by molecular diffusion.

The analogous treatment of laminar falling film condensation by Sparrow and Gregg (*28*) showed that acceleration terms and heat convection terms could be neglected as long as the Prandtl number N_{Pr} was above 0.1 and the evaporation number $N_{Ev} = c(T_o - T_{ev})/\lambda$ was below 2.0. For water at 212°F., with $T_o - T_{ev}$ even as high as 50°F., N_{Ev} is about 0.05 and N_{Pr} is 1.7. At lower temperatures and/or higher salinities, N_{Pr} is even higher and N_{Ev} lower. Thus in the present case the governing equations are

$$\frac{\partial u}{\partial x} + \frac{\partial v}{\partial y} = 0 \tag{1}$$

$$0 = g + \nu \frac{\partial^2 u}{\partial^2 y} \tag{2}$$

$$0 = a \frac{\partial^2 T}{\partial y^2} \tag{3}$$

$$u \frac{\partial S}{\partial x} + v \frac{\partial S}{\partial y} = D \frac{\partial^2 S}{\partial y^2} \tag{4}$$

The boundary conditions are (see Figure 2)

Inlet (uniform flow)

$$x = 0: \quad h = h_i;\ u = u_i = m_F/\rho h_i;\ T = T_{ev};\ S = S_F \tag{5}$$

Wall (no slip)

$$y = 0: \quad u = 0;\ v = 0;\ T = T_o;\ \partial S/\partial y = 0 \tag{6}$$

(zero salt diffusion across wall)

Free surface (zero shear)

$$y = h: \quad \frac{\partial u}{\partial y} = 0;\ T = T_{ev} \tag{7}$$

$$-k \frac{\partial T}{\partial y} = -\lambda \frac{dm}{dx} \tag{8}$$

(free surface heat balance)

$$\rho D \frac{\partial S}{\partial y} = -S \frac{dm}{dx} \tag{9}$$

(zero nonvolatile solute flow across free surface)

$$-\frac{dm}{dx} = \rho \left(v_h - u_h \frac{dh}{dx} \right) \tag{10}$$

(mass flow across free surface)

The inlet condition $u = u_i$ rapidly changes to satisfy Equation (2). For isothermal films the momentum start-

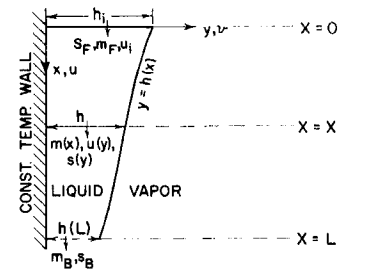

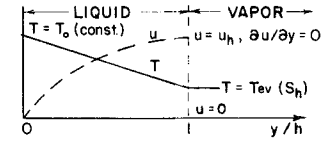

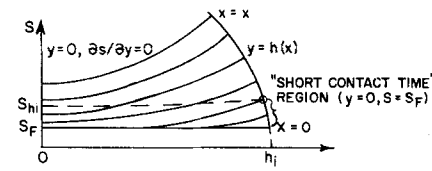

Fig. 2. (*a, top*) Falling film analysis model. (*b, middle*) Qualitative developed temperature and velocity profiles. (*c, bottom*) Qualitative salinity profiles.

ing length has been shown to be of the order of ten film thicknesses and therefore negligible (*13, 20*). Integration of Equations (2) and (3) gives a parabolic velocity profile and a straight line temperature distribution. Equation (8) then integrates (with $m = m_F$ at $x = 0$) to

$$m = m_F (1 - A'x)^{3/4} = m_F r^{3/4}; \quad r = 1 - A'x \qquad (11)$$

The associated result for film thickness is

$$h = h_i r^{1/4} \qquad (12)$$

which was obtained by Linke (*19*). For a pure liquid evaporation is complete when $m = 0$, that is, when $x = 1/A'$. For a salt solution, salt flow is conserved, that is, from Equation (11)

$$S_{Av}(x) = S_F \frac{m_F}{m(x)} = S_F r^{-3/4} \qquad (13)$$

The evaporated fraction $m_{ev}/m_F = (m_F - m)/m_F$ from Equation (11) is

$$\frac{m_{ev}}{m_F} = 1 - \left\{1 - \left[4\left(\frac{\pi}{3}\right)^{4/3} g^{1/3} L d^{4/3}\right] \psi \frac{\Delta T}{M_F^{4/3}}\right\}^{3/4} \qquad (14)$$

The salinity profile is evaluated in the Appendix. Figure 3 is a plot of the ratio of free surface salinity to average film salinity S_h/S_{av} vs. the dimensionless "salinity profile number" B. Over the range of interest, S_h/S_{av} does not exceed 1.25, and a value of 1.1 is a good average. This result means that the experimental falling film salinity profiles are expected to be approximately flat. This deduction is based on a molecular diffusion rate, and, if the diffusion rate is higher owing to an eddy contribution, the profile will be even flatter.

Variable Property Laminar Model

The effect of boiling point elevation (B.P.E.) on evaporation temperature difference is the most significant variable property effect. Therefore, an approximate variable property solution accounting for the B.P.E. effect was derived.

The B.P.E. is assumed to be a power function, and the free surface salinity is taken as 1.1 times the average value:

$$\Delta T_{BPE} = \alpha S_h^{\beta} \qquad (15)$$

$$S_h = S_{av}(S_h/S_{av}) = 1.1 S_F m_F/m \qquad (16)$$

A power function fit for ΔT_{BPE} has been found applicable (*33*). The quantity S_h is found from Equation (13), with the factor 1.1 based on an average for S_h/S_{av} from Figure 3. The temperature difference across the film ΔT is then given (at any x) by

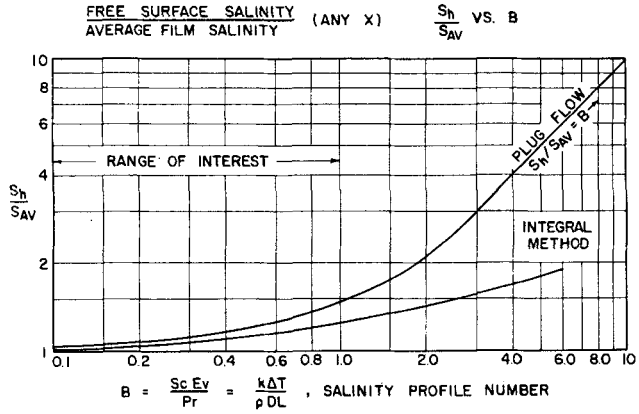

Fig. 3. Comparison of falling film salinity solutions.

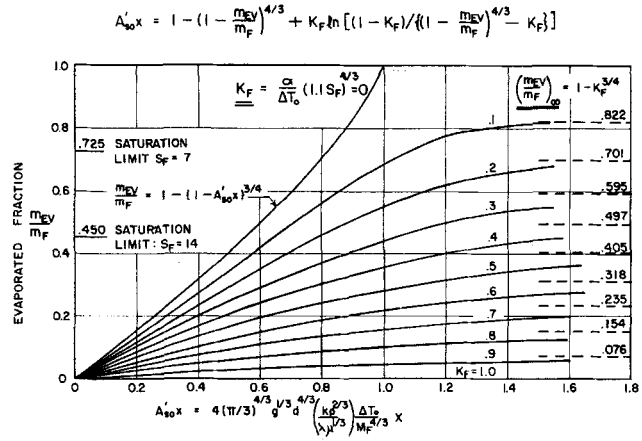

Fig. 4. Laminar falling film evaporation with boiling point elevation $\Delta T_{BPE} = \alpha S^{4/3}$.

$$\Delta T = T_o - (T_{so} - \Delta T_{BPE}) = T_o - \alpha (1.1 S_F m_F)^{\beta} m^{-\beta} \qquad (17)$$

When this expression for ΔT is inserted into the basic laminar evaporation Equation (8), and the integration is carried out, after rearranging there results

$$A'_{so}x = \int_{(m/m_F)^{4/3}}^{1} \frac{d\left[\left(\frac{m}{m_F}\right)^{4/3}\right]}{1 - K_F\left[\left(\frac{m}{m_F}\right)^{4/3}\right]^{-3\beta/4}} \qquad (18)$$

where

$$A'_{so}x = A'x \frac{\Delta T_o}{\Delta T} = 4\left(\frac{\pi}{3}\right)^{4/3} g^{1/3} x d^{3/4} \psi \Delta T_o M_F^{-4/3} \qquad (19)$$

$$K_F = \frac{\alpha}{\Delta T_o}(1.1 S_F)^{4/3} \qquad (20)$$

In the B.P.E. power law take $\beta = 4/3$ and $\alpha = 0.153$, making the deviations from the experimental B.P.E. curve (*33*) within 0.2°F. over the S range from 1 to 20%.

This approximation then simplifies the integral in Equation (18) to a form which is readily integrable:

$$A'_{so}x = \int_t^1 \frac{dt}{1 - K_F t^{-1}}; \quad t = \left(\frac{m}{m_F}\right)^{4/3} \qquad (21)$$

$$A'_{so}x = 1 - \left(1 - \frac{m_{ev}}{m_F}\right)^{4/3} + K_F \ln \frac{1 - K_F}{\left(1 - \frac{m_{ev}}{m_F}\right)^{4/3} - K_F} \qquad (22)$$

This quantity is graphed for different values of K_F on a plot of m_{ev}/m_F vs. A'_{so} x in Figure 4. The abscissa involves only known inputs, with the exception of the property grouping ψ which is to be taken at an x averaged "mean" salinity S. The parameter K_F is the fraction of ΔT_o already unavailable in the feed due to B.P.E.; if $K_F = 1$, no evaporation at all can occur, regardless of A'_{so} x. Otherwise, evaporation increases with A'_{so} x to an asymptotic limit shown in Figure 4.

If it is desired to design the evaporator such that no salt precipitation occurs, the free surface salinity S_h must be limited to the saturation value of close to 28%. Then, from Equation (16)

$$\left(\frac{m_{ev}}{m_F}\right)_{sat} = 1 - \frac{1.1 S_F}{28} \qquad (23)$$

For $S_F = 7$ and 14, these saturation-limited evaporating fractions are 0.725 and 0.450, respectively.

For given S_F and K_F values, which determine corresponding values of $(m_{ev}/m_F)_{sat}$ and $(m_{ev}/m_F)_\infty$, respectively, Figure 4 exhibits three evaporation regimes found experimentally:

1. "Total, fully wetted" evaporation when m_{ev}/m_F lies below $(m_{ev}/m_F)_{sat}$ and below $(m_{ev}/m_F)_\infty$.
2. "Partial, fully wetted" evaporation when m_{ev}/m_F lies below $(m_{ev}/m_F)_{sat}$, but $A'_{so}\ x$ is large enough so that $(m_{ev}/m_F)_\infty$. Here the surface is fully wetted, the salinity everywhere below saturation, but the temperature difference across film is zero (no evaporation) over the lower part of the surface, where the B.P.E. has risen to a high enough value.
3. "Total, partly precipitated" evaporation when m_{ev}/m_F lies above $(m_{ev}/m_F)_{sat}$, but below $(m_{ev}/m_F)_\infty$. Here the lower part of the surface has a salinity above saturation, and there is a mixture of saturated liquid solution and salt precipitate. The temperature difference must exceed the B.P.E. at saturation, which is about 15°F. for sodium chloride solution.

EXPERIMENTAL APPARATUS AND PROCEDURES

Evaporator

A cross section through the evaporator is shown in Figure 5. The stationary vertical copper heat transfer tube, nominally 4 in. O.D., 0.25 in. wall thickness and 16 in. long, is heated internally by condensing steam. A 9-in. I.D. glass pipe, through which evaporation may be observed all around the copper tube, seals the evaporator together with an upper and lower stainless steel plate. An electrically heated conducting and 75% transparent coating deposited on the outside of the glass prevents condensation of yield vapor on the inside of the glass pipe. The yield vapor is drawn off through a duct at the top of the evaporator into a separate yield condenser. The concentrated brine flows down the vertical copper surface to form a pool which empties through the bottom evaporator plate. Similarly, the condensed steam flows down through the steam pipe out of the evaporator.

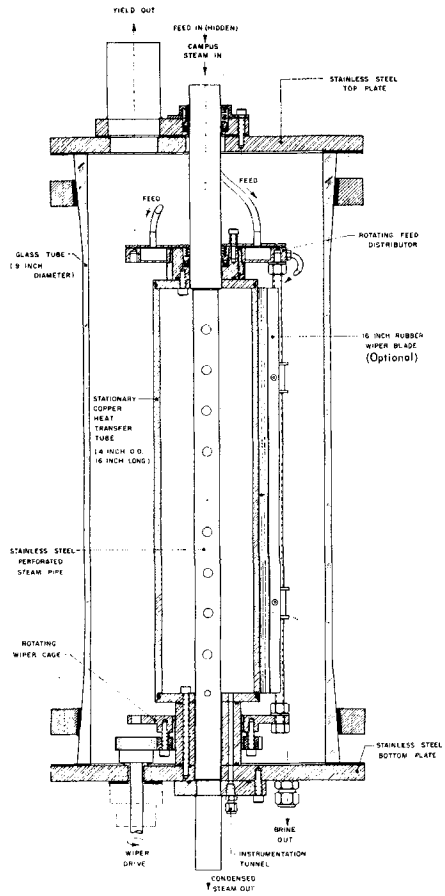

Fig. 5. Evaporator cross section.

Above the tube there is a rotating cylindrical feed reservoir concentric with the tube, attached to a cage driven from below by a variable speed drive. The saline feed water flows through the rotating reservoir onto the copper surface under gravity through six feed ducts. Tests indicated that a uniform falling film was achieved when the ducts were oriented radially inward normal to the copper surface and the rotation was in excess of 90 rev./min. so the feed duct rotation for the falling film evaporation runs was fixed at 120 rev./min.

For heat transfer measurement purposes, the copper tube is provided with five wall thermocouples in a vertical line. Figure 6 illustrates the nature of the thermocouple insertion.

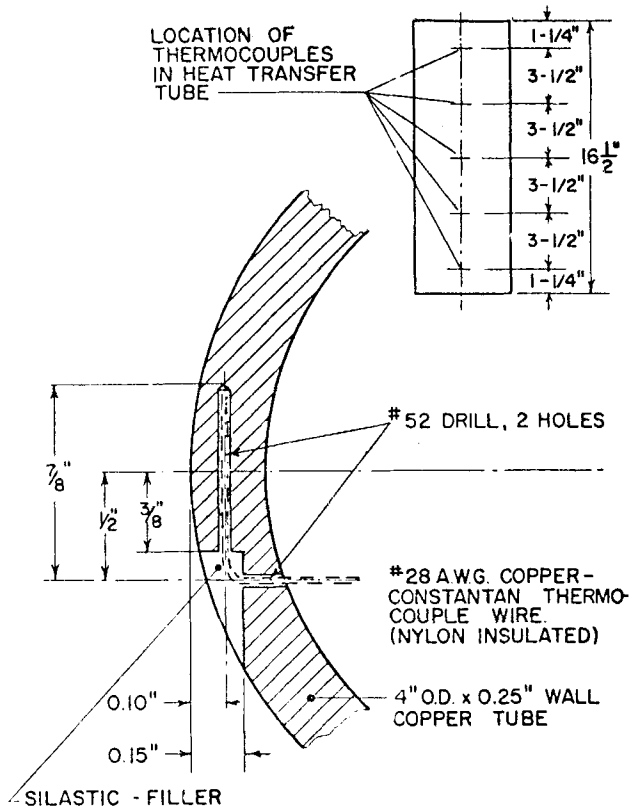

Fig. 6. Instrumentation of heat transfer tube.

Distillation System

A flow diagram of the entire distillation system appears as Figure 7. The feed system is of the batch type, with flows up to 100 lb./hr. An 80-gal. stainless steel feed-water deaeration and heating tank is charged with pure water or saline water (aqueous sodium chloride solution) of desired feed salinity. A 10-kw. immersion heater brings the feed water batch to a boil, driving off inerts in the feed water through a vent. Vigorous boiling overnight provides hot deaerated feed water. A pump, control valve and trim heater, provide the desired feed temperature (a degree or two below the boiling point) and flow rate to the rotating reservoir.

Low pressure steam with a controlled amount of superheat (typically 10°F.) is provided at entry to the condensation side of the evaporator. Provision exists for injecting a dropwise condensing promoter into the steam line ahead of the evaporator. The steam condenses on the inside of the copper tube and then flows into an insulated sump.

From the evaporator upper plate the evaporated yield vapor passes through a wire mesh droplet eliminator and a 2-in. duct into a separate insulated external water-cooled yield condenser, with control of evaporation pressure through adjustment of condenser cooling water flow. The evaporator and yield condenser pressures are within 0.05 lb./sq. in. of each other.

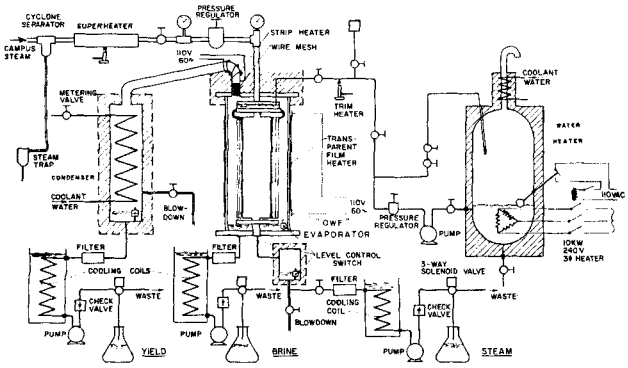

Fig. 7. Distillation system flow diagram.

The liquid levels in the yield condenser, brine pool, and steam condensate sump are maintained within close limits by automatic magnetic float switches which effect periodic pumping of these streams into measuring vessels. Each stream is cooled to room temperature before collection to eliminate evaporation losses. Check valves in all circuits permit operation of the distillation system at less than atmospheric pressure.

Instrumentation

Temperatures were measured with calibrated thermocouples to 0.2°F. Water vapor and steam pressures were read on mercury manometers made of ½ in. O.D. transparent nylon tubing, taking into account condensed water above the mercury.

The feed flow rate was measured by a commercial sharp-edged orifice installation leading to a flow integrator, and calibrated over the experimental range of flows. The brine, yield, and steam flow rates were obtained from volumes collected in the measuring vessels over known time periods. The feed and brine salinities were measured by hydrometer and electrical conductivity cell. The latter was also used to establish the yield purity.

Evaporation Runs

After flow and thermal equilibrium at various input conditions were established data were taken from which steady state evaporation performance was calculated. A wetting copper evaporation surface was obtained by adding to the feed water: (1) H-400 sulfamic acid scale solvent, and (2) a saturated solution of ammonium carbonate in ammonium hydroxide.

Next, 2 cc. of a dropwise promoter, 10% solution of Montan wax in liquid petrolatum, was injected into the steam (*34, 35*). During a half-hour steaming period for good distribution of the promoter on the condensing surfaces, the steam and feed flows and temperatures were adjusted, the steam and yield systems were blown down to purge them of air, and the heating of the glass pipe was set at the point where condensation on the inside of the tube just stopped.

Data Reduction

A wetted-area-weighted-averaging procedure was used in the data reduction to obtain an effective constant heating surface temperature. Condensation and evaporation temperature differences were based on the assumption that the steam or vapor temperature was that corresponding to saturation at the measured steam or vapor pressure. The heat for evaporation was taken as the difference in enthalpy between the incoming superheated steam and the outgoing steam condensate. The inside and outside wall temperatures of the copper tube were obtained from the wall temperature measurements with the assumption of radial heat flow through the copper tube. The outer surface of the liquid film was the boundary of the control volume for heat and mass balances, in which flow rates and enthalpy rates of all streams were considered.

The entire data reduction from raw data to performance variables was carried out by means of an IBM 7090 digital computer program containing analytical expressions for all calibrations, properties, and functions in terms of temperature, pressure, salinity, etc. The equations, detailed procedural steps, and the Fortran listing of the program are found in reference *36*.

DISCUSSION OF RESULTS

Ranges and Validity of Experiments

Runs were carried out for all combinations of three salinities (0, 7, and 14%, that is, zero, two, and four times sea water concentration) and three feed flow rates (nominally 45, 70, and 95 lb./hr.). At each of these nine conditions, the variable was evaporation temperature difference which was increased from 1.7° to 18.3°F. The observed evaporated fraction varied correspondingly from 1 to 64%. The feed flow Reynolds number varied from 159 to 596, the Prandtl number ranged from 1.6 to 2.2, and B ranged from 0.025 to 0.541.

The internal consistency of the data was checked by making mass and heat balances. Errors were predominantly in the direction of losses from the system, the median and maximum errors being 1.75 and 5.5% for mass and 5.5 and 15.5% for heat balances. These figures are typical of evaporator operation and are considered to be a satisfactory validation of the results.

Evaporation Mechanism

Even at the highest evaporation temperature differences, there were always less than ten active nucleate bubble sites over the whole copper tube, and the free surface was at all times smooth and specularly reflecting. The straight vertical motion of the few bubbles showed that the rotating feed ducts did produce a falling film. Jakob (*15*) assigned a heat transport of 59 B.t.u./hr. to each bubble column, so that the few bubbles had virtually no effect on the evaporation. The mechanism must be considered to be surface evaporation.

Falling Film Continuity

It was found that the presence or absence of evaporation and of salt in the falling film had a pronounced effect on the tendency of the film to break up into channels or rivulets. With the glass pipe of the evaporator removed for better photographic visibility, 16-mm. movies were taken.

When no evaporation was taking place and cold feed water was introduced in the form of a falling film, a smooth, glassy, fully-wetted copper tube surface resulted. When the tube was steam-heated to produce evaporation of a pure water falling film, ripples of increasing amplitude appeared in the film with increase in temperature difference, until the falling film broke up into irregular channels.

When 7 or 14% saline water was substituted for the pure water, ripples were still present at comparable conditions, but much less so than for pure water. The falling film remained continuous regardless of the temperature difference.

These phenomena can be explained qualitatively by the effect of temperature and salinity on surface tension gradients which give rise to surface movements. Norman and Binns (*21*) explained the instability of an evaporating pure water film by noting that the film surface is actually rippled from a number of causes so that the film thickness is perturbed locally. In the nonequilibrium situation, thin film areas have a higher temperature than thick areas and therefore, with pure water, a lower surface tension. The result is that liquid is drawn from the thin to the thick film areas, causing breakup. With increasing temperature difference, the film becomes thinner throughout and breakup should become more severe, as was observed.

Under comparable variable thickness conditions, a saline film has a higher surface salinity in the thinner areas, which causes a higher surface tension there, because the

increase of surface tension with salinity tends to outweigh any decrease of surface tension with increase in temperature. Thus should a thin spot occur, there is a surface force tending to draw liquid from the thicker to the thinner regions.

For a given pressure (or temperature) difference, a reduction in pure water feed flow rate from $M_F = 90$ to $M_F = 20$ results in progressively greater breakup of an initially continuous film into discrete channels or rivulets. These observations are in qualitative agreement with the minimum wetting rate data found by Norman and coworkers (*21, 22*).

Salt Effects Other Than Boiling Point Elevation

The use of acid and ammonia solutions as feed water additives produced a pinkish virgin copper surface by removing any accumulated oxide scale. Subsequent dry exposure to the room environment produced a light brown oxide tarnish evenly around the tube.

When the feed water was switched to 7 or 14% deaerated hot (in excess of 150°F.) saline water, the tarnish on the copper surface was removed and the virgin condition restored in about 10 min. of evaporation.

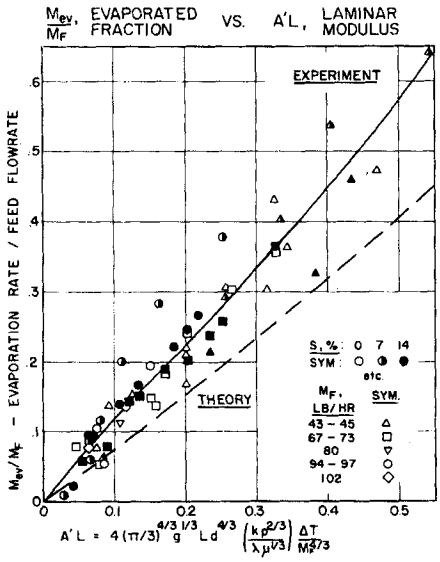

Fig. 8. Falling film evaporation. Comparison with laminar evaporation analysis.

An increase in temperature (pressure) difference was observed to change the evaporation regime of saline water from fully wetted to partly precipitated. In the latter condition salt began to precipitate around the bottom of the tube and consisted of very grainy crystals of uneven thickness. Snowflakelike surface patterns were observed, and in many places liquid continued to flow down beneath the surface layer of salt crystals. Throughout all evaporation experiments, the yield sodium chloride content was less than 50 p.p.m., the lower limit of the conductivity cell used.

Evaporation Data

A comparison between the experimental data and the constant property laminar analysis is seen in Figure 8. For the experimental range of feed flow Reynolds numbers (roughly 160 to 600), the laminar modulus arising out of the constant property evaporation analysis provides a means of correlating the experimental evaporation data. The mean experimental line corresponds to evaporation rates which are between 40 and 60% above those predicted by constant property laminar theory. Another comparison was made with the variable property laminar analysis. Since B.P.E. reduces predicted evaporation, the average experimental rates exceeded the prediction by 70%.

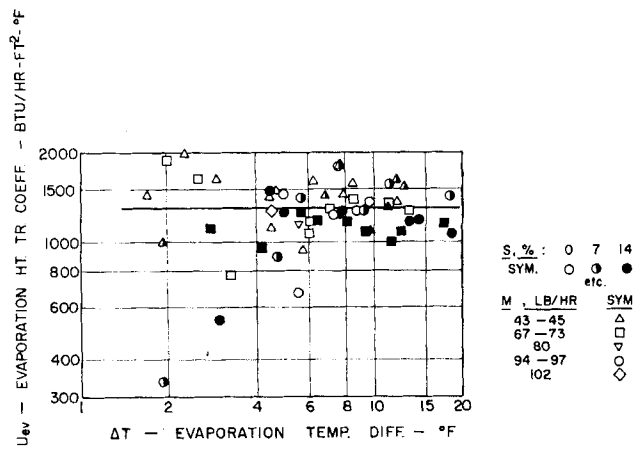

Fig. 9. Falling film evaporation. Heat transfer coefficient vs. temperature difference.

The falling film evaporation heat transfer coefficients are plotted against ΔT in Figure 9 for all data points. Most of the points lie in the range between 1,100 and 1,600 B.t.u./(hr.)(sq. ft.)/°F. (average value 1,300) with no noticeable effects due to salinity, feed flow rate, or ΔT. The absence of a ΔT effect would be expected, based on the simplified expression k/h for the evaporation coefficient which then only depends on film thickness. The absolute magnitude of the coefficients is comparable to that observed by other investigators who used pure water in the liquid state as feed over a similar range of evaporation temperature differences (*4, 26*).

The heat transfer coefficients were put into nondimensional form in accordance with the "eddy" treatment and plotted against average Reynolds number (see Figure 10). The dashed lines give predicted laminar ($U = k/h_{lam}$) and eddy heat transfer. The band enclosed between the two eddy lines corresponds to the experimental Prandtl number range of 1.6 to 2.2 at 15 lb./sq. in. abs. The solid curve correlates the experimental results within plus or minus 20% and lies above both theoretical curves.

Condensation Data

Condensation coefficients varied from 2,000 to 10,000 B.t.u.(hr.)(sq. ft.)/°F., with an average value of 4,550. For comparison the calculated theoretical laminar film condensation coefficient (Nusselt, 23) varied from 1,700 to 3,000 over the experimental range of temperature dif-

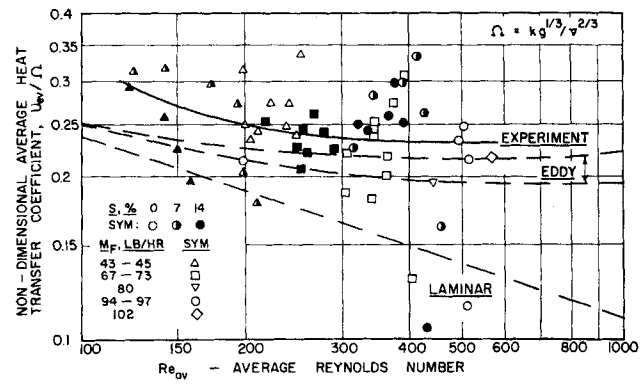

Fig. 10. Falling film evaporation. Heat transfer coefficient comparison with eddy and laminar analyses.

ferences. With clean copper surfaces, the use of Montan wax injection produced larger gains in condensation coefficient (24).

CONCLUSIONS

Analysis

1. A laminar saline water falling film evaporation analysis accounting for B.P.E. (the principal variable property effect) realistically predicts: total, fully wetted; partial, fully wetted; or total, partly precipitated evaporation regimes, depending on temperature difference and feed salinity (Figure 4).

2. The salinity variation across the evaporating film, dependent on the dimensionless number B, is small, typically 10% (Figure 3).

Experiment

1. The mechanism of free surface evaporation was observed at all test conditions with liquid, nonboiling feed.

2. Film continuity was poor for pure water but good for saline water. This may be explained by the influence of temperature and salinity on surface tension gradients.

3. Evaporation rates from falling saline water films in the laminar transitional regime (feed Reynolds number from 160 to 600) at atmospheric pressure, with variable feed salinity (0 to 14%) and temperature difference (up to 18°F.) could be correlated by the dimensionless laminar modulus $A'x$ and by the dimensionless heat transfer coefficient U_{ev}/Ω.

4. The mean line of the evaporation results lies 40 to 70% above the laminar analyses and 12% above the eddy treatment. In view of the possibility of additional turbulence in the feed from the rotating distributor, the results are considered to be in good agreement with the eddy treatment.

ACKNOWLEDGMENT

This work was supported by the State of California through the Statewide Water Resources Center. Professors J. W. McCutchan and R. L. Perrine acted as Program Coordinator and Project Leader, respectively. R. M. Webb collaborated in the experiment and W. Gregson, Jr., in the design of the evaporator.

NOTATION

A' = $4(4/3)^{4/3}\ (N_{Ev}/N_{Pr})\ N_{ReF}^{-4/3}\ g^{1/3}\ \nu^{-2/3} = 4(\pi/3)^{4/3}\ g^{1/3}\ d^{4/3}\ \psi\ \Delta T\ M_F^{-4/3}$, ft.$^{-1}$

A'_{so} = $A'\Delta T_o/\Delta T$, ft.$^{-1}$

$A'x$ = laminar modulus ($A'L$ for evaporator), dimensionless

a = thermal diffusivity, sq. ft./hr.

B = salinity profile number, $N_{Sc}(N_{Ev}/N_{Pr}) = k\Delta T/D\rho\lambda$, dimensionless

c = specific heat, B.t.u./(lb.$_m$)(°F.)

D = molecular diffusion coefficient, sq. ft./hr.

d = diameter of evaporation surface (O.D. of heat transfer tube), ft.

g = acceleration of gravity on earth's surface, 4.17×10^8 ft./hr.^{2}

h = liquid film thickness (y direction), ft.

K_F = $(\alpha/\Delta T_o)\ (1.1\ S_F)^{4/3}$, dimensionless

k = thermal conductivity, B.t.u./(ft.)(hr.)/°F.

L = height of evaporator, ft.

M = mass flow rate, lb./hr.

m = mass flow rate per unit horizontal width, $M/\pi d$, lb./(hr.)(ft.)

N = dimensionless number

r = $1 - A'x$, dimensionless

S = salinity, 100 mass of solids/mass of mixture, %

T = temperature, °F. or °R.

T_{ev} = evaporation temperature, saturated vapor at P_{ev} and $S = S_h$, °F. or °R.

T_o = temperature of evaporation surface (O.D. of heat transfer tube), °F. or °R.

T_{so} = salinity zero temperature, saturated vapor at P_{ev} and $S = 0$ (pure water), °F. or °R.

U = heat transfer coefficient B.t.u./(hr.)(sq. ft.)/°F.

u = vertical axial velocity (x direction), ft./hr.

v = horizontal radial velocity (y direction), ft./hr.

x = vertical axial coordinate ($x = 0$ at top, $x = L$ at bottom of evaporator), ft.

y = horizontal radial coordinate ($y = 0$ at heating surface, $y = h$ at free film surface), ft.

Greek Letters

α,β = coefficients in $\Delta T_{BPE} = \alpha S_h^{\beta}$

ΔT = evaporation temperature difference, $T_o - T_{ev}$, °F.

ΔT_{BPE} = boiling point elevation, °F.

ΔT_o = zero salinity temperature difference, $T_o - T_{so}$, °F.

Λ = y/h, dimensionless

λ = latent heat of vaporization, B.t.u./lb.

μ = absolute (dynamic) viscosity, lb.$_m$/(ft.)(hr.)

ν = kinematic viscosity, sq. ft./hr.

ρ = mass density, lb.$_m$/cu. ft.

ψ = properties group $k\rho^{2/3}/\lambda\mu^{1/3}$, ft.$^{-8/3}$ lb.$_m^{4/3}$ hr.$^{-2/3}$ °F.$^{-1}$

Ω = properties group $kg^{1/3}/\nu^{2/3}$, B.t.u./(hr.)(sq. ft.)/°F.

Subscripts

av = average

B = brine

B.P.E. = boiling point elevation

C,c = condensing, condensation, condensate

Ev = evaporation $N_{Ev} = c\Delta T/\lambda$

ev = evaporated, evaporation, evaporating

F = feed, inlet

h = free surface of liquid film ($y = h$)

i = film at $x = 0$; initial

lam = laminar

o = evaporation surface ($y = 0$); zero salinity

Pr = Prandtl, $N_{Pr} = \nu/a$

Re = Reynolds, $N_{Re} = 4m/\mu$

Sc = Schmidt, $N_{Sc} = \nu/D$

x = at x coordinate

LITERATURE CITED

1. Asbjørnsen, O. A., *Chem. Eng. Sci.*, **14**, 211-226 (1961).
2. Bressler, R., *Ver. Deutscher Ing. Zeit.*, **100**, 630-638 (1958).
3. ———, *Forschungsbericht No. 770*, Kultusministerium Nordrhein-Westfalen, Cologne (1960).
4. Broker, B., and J. W. McCutchan: *Dept. of Eng. Univ. California, Los Angeles, Rept. No. 60-58* (July, 1960).
5. Collier, J. G., *Trans. Inst. Chem. Engrs. (London)*, **38**, No. 6, 320-321 (1960).
6. ———, and G. F. Hewitt: *Rept. AERE R4684*, UKAEA, Harwell, England (July, 1964).
7. DeGroot, S. R., "L'Effet Soret—Diffusion Thermique dans les Phases Condensées," North Holland Publishing Co., Amsterdam (1945).
8. DeGroot, S. R., "Thermodynamics of Irreversible Processes," Interscience, New York (1952).
9. Deissler, R. G., *Natl. Advisory Comm. Aeronaut. Tech. Note 2129*, (1950); *2138* (1952); *3145* (1959).
10. Dukler, A. E., *Chem. Eng. Progr. Symposium Ser. No. 30*, **56**, 1-10 (1960).
11. ———, *Am. Rocket Soc. J.*, **31**, 86 (1961).

12. Greenberg, A. B., Ph.D. thesis, Purdue Univ., Lafayette, Ind. (1956).
13. Hasselgruber, H, Diploma thesis, Tech. Hochschule Aachen (1950), (quoted by Linke, 19).
14. Hsu, Y. Y., F. F. Simon, and J. F. Lad, *Chem. Eng. Progr. Symposium Ser. No. 57*, **61** (1965).
15. Jakob, M., "Heat Transfer," Vol. 1, p. 627, Wiley, New York (1949).
16. Kapitsa, P. L., *Zhur. Eksp. Teor. Fiz. (JETP)*, Pt. 1, **18**, 3-28 (1948).
17. Karetnikov, U. P., *Zhur. Tekhn. Fiziki*, Pt. 2, **24**, 193-199 (1954).
18. Keville, J. F., *Chem. Eng. Progr.*, **54**, No. 10, 83-84 (October, 1958).
19. Linke, W., *Kältetechnik*, **5**, No. 10, 275-279 (1953).
20. Lynn, S., *A.I.Ch.E. J.*, **6**, No. 4, 703-705 (1960).
21. Norman, W. S., and D. T. Binns, *Trans. Inst. Chem. Engrs. (London)*, **38**, No. 6, 294-300; *discussion*, 317-323 (1960).
22. Norman, W. S., and V. McIntyre, *ibid.*, 301-307, *ibid.*
23. Nusselt, W., *Ver. Deutscher Ing. Zeit.*, **60**, 541-546, 569 (1916).
24. Osment, B. D. J., and D. W. Tanner, *Natl. Eng. Lab. Rept. No. 34*, East Kilbride, Glasgow, Scotland, also *Dechema Monographien*, **47**, No. 781-804, 145-174, Verlag Chemie, Weinheim/Bergstrasse, Germany (1962).
25. Portalski, S., Ph.D. thesis, Univ. London, England (1960).
26. Richkov, A. I., and V. K. Pospelov, *Khim. Prom. (Chem. Ind.)*, **5**, 426-429 (1959).
27. Sinek, J. R., and E. H. Young, *Chem. Eng. Progr.*, **58**, No. 12, 74-80, (December, 1962).
28. Sparrow, E. M., and J. L. Gregg, *J. Heat Transfer*, **81**, 13-18 (February, 1959).
29. Standiford, Jr., F. C., and H. F. Bjork, *Advanc. Chem. Ser.*, No. 27, 115-127 (1960).
30. Tailby, S. R., and S. Portalski, *Trans. Inst. Chem. Engrs. (London)*, **38**, No. 6, 324-330 (1960).
31. ———, *Chem. Eng. Sci.*, **17**, 283-290 (1962).
32. Unterberg, Walter, *Dept. Eng. Univ. California, Los Angeles, Rept. No. 61-26* (October, 1961).
33. ———, *Dept. Eng. Univ. California, Los Angeles, Rept. No. 64-21* (May, 1964).
34. Watson, R. G. H., J. J. Brunt, and D. C. P. Birt, *International Developments in Heat Transfer*, Part II, Paper 35, 296-301, Amer. Soc. Mech. Engrs., New York (1961).
35. Watson, R. G. H., Admiralty Materials Lab., Poole, England, private communication (1962).
36. Webb, R. M., W. Unterberg, and W. Gregson, Jr., *Dept. Eng. Univ California, Los Angeles, Rept. No. 64-23* (August, 1964).

APPENDIX 1: SALINITY PROFILES IN LAMINAR FLOW

Diffusion Equation and Boundary Conditions

The diffusion equation and boundary conditions whose solution yields the salinity profile across the evaporating film are Equations (4), (5), (6), and (9). By use of the straight line temperature profile and the definition of B, Equation (9) can be transformed to

$$y = h: \frac{\partial S}{\partial y} = \frac{BS}{h} \tag{24}$$

In these equations u and v are known functions of (x, y) from the parabolic velocity distribution and continuity, and h is a known function of x from Equation (12). The substitution for h, u, and v in terms of x and y permits Equation (4) to be written

$$\left[8h_i r^{1/4} y - 4y^2 \right] \frac{\partial S}{\partial x} + \left[A' h_i r^{-3/4} y^2 \right] \frac{\partial S}{\partial y} = \left(\frac{8\nu D}{g} \right) \frac{\partial^2 S}{\partial y^2} \tag{25}$$

Plug Flow Salinity

For an approximate solution one may consider the velocity constant across the film, for example, at the value u_h. The film thickness varies slowly with x and may also be taken as constant to begin with. The diffusion equation is then solved for constant u and h, and a quasistationary solution is obtained by later inserting the known variation of u_h and h with x. While the boundary conditions Equations (6) and (24) are unchanged, the equation and inlet condition become

$$u \frac{\partial S}{\partial x} = D \frac{\partial^2 S}{\partial y^2} \tag{26}$$

$$x = o: S_{av} = \frac{1}{h_i} \int_o^{h_i} S \, dy \tag{27}$$

The inlet condition, Equation (27), has been written in terms of an average salinity across the film.

A solution by separation of variables is tried and the three boundary conditions, Equations (27, 6, 24), are applied with the result

$$\frac{S}{S_F} = \frac{\phi^2}{B} \exp\left(\frac{D\phi^2 x}{h^2 u} \right) \frac{\cosh(\phi y/h)}{\cosh \phi} \tag{28}$$

where

$$\phi \tanh \phi = B \tag{29}$$

$$\frac{S_h}{S_{av}} = \frac{S_h/S_F}{S_{av}/S_F} = \frac{(\phi^2/B)\, f(x)}{\int_o^1 (S/S_F)\, d(y/h)} = \frac{\phi^2}{B} = f(B) \tag{30}$$

General Salinity

To obtain a solution of the complete salinity Equation (25), an approach is taken which considers the fully developed salinity profiles in the y direction to be "similar" at all x, according to

$$S = S_h(x)\, G(\Lambda) \tag{31}$$

The second-order salt conservation equation has two boundary conditions which apply to G, one at the wall and one at the free surface:

$$G'(0) = 0 \quad \text{equivalent to Equation (6)} \tag{32}$$

$$G(1) = 1 \quad \text{by inspection from Equation (31)} \tag{33}$$

The Karman-Polhausen integral method for boundary-layer problems may be applied here by taking the profile function $G(\Lambda)$ in Equation (31) as a specified function with undetermined coefficients which are found by fitting the function to the salinity Equation (25) when integrated across the film and by meeting the boundary conditions. The result for integration up to y_a, $y_a < h$, is

$$\int_o^{\Lambda} F G \, d\Lambda + 2G(\Lambda_a) \int_o^{\Lambda_a} F \, d\Lambda = \frac{2}{B} G'(\Lambda_a) \tag{34}$$

where

$$F(\Lambda) = 2\Lambda - \Lambda^2 \tag{35}$$

The choice of a profile for $G(\Lambda)$ is based on the previous plug flow solution which indicates that the salinity profile is very flat from the wall out to a point closer to the free surface than to the wall, and then rises more steeply to its maximum value at the free surface, as shown in the profile

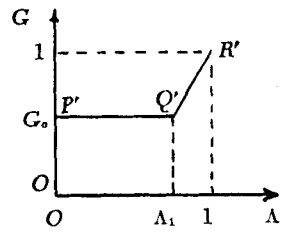

This profile consists of a horizontal part $P'Q'$ at a value G_o from the wall to a point $\Lambda = \Lambda_1$, and a linear part $Q'R'$ from $\Lambda = \Lambda_1$ to $\Lambda = 1$, with a slope $G'(1) = R$. Inspection of the sketch reveals that both boundary conditions, Equations (32) and (33), are satisfied, and that the profile is determined when the three unknowns, G_o, Λ_1, and R, are found. The three

necessary equations are obtained from: (1) the goemetrical relationship among G_o, Λ_1, and R; (2) evaluation of Equation (34) with $\Lambda_a = \Lambda_1$, and (3) evaluation of Equation (34) with $\Lambda_a = 1$.

In evaluating Equation (34) over the horizontal part of the profile, the slope $G'(\Lambda_1)$ is taken as the average of the slopes of the lines meeting at $\Lambda = \Lambda_1$, that is, $G'(\Lambda_1) = R/2$. When G_o and R are eliminated from these equations, Λ_1 is given by the implicit relation

$$\frac{1 - (3\Lambda_1^2 - \Lambda_1^3)^{-1}}{(7/8) - \Lambda_1 + (1/6)\,\Lambda_1^3 - (1/24)\,\Lambda_1^4} = B \qquad (36)$$

Numerical answers are obtained by evaluating B in Equation (36) for different input values of Λ_1. For a known set of Λ_1 and B, the quantity R is found, and the salinity ratio of interest becomes

$$S_h/S_{av} = [(3R/B) - 2]^{-1} \qquad (37)$$

The following tabulation gives the numerical results (slide rule accuracy):

B	Λ_1	R/B	S_h/S_{av}
0.074	0.66	0.994	1.020
0.177	0.67	0.986	1.042
0.284	0.68	0.980	1.070
0.509	0.70	0.961	1.130
1.154	0.75	0.926	1.282
2.02	0.80	0.897	1.447
5.97	0.90	0.845	1.887

It is seen that the Λ_1 values lie in the third of the film thickness which is closest to the free surface, and that the gradient of G at the free surface, R, is close to B and approaches B as B approaches zero.

Manuscript received February 23, 1965; revision received June 7, 1965; paper accepted June 8, 1965. Paper presented at A.I.Ch.E. Houston meeting.

Direct Contact Heat Transfer with Change of Phase:

Effect of the Initial Drop Size in Three-Phase Heat Exchangers

SAMUEL SIDEMAN, GIDEON HIRSCH, and YEHUDA GAT

Technion, Israel Institute of Technology, Haifa, Israel

The initial drop size of volatile fluids evaporating within immiscible, nonvolatile liquids was experimentally related to the overall heat transfer coefficient in single and multiparticle systems. Coalescence and turbulence diminish the effects of the initial size, which are thus limited to the lower part of the exchanger where single-drop characteristics are maintained. Condensation data of single bubbles are in good agreement with the single-drop relationship.

The problem of direct-contact heat exchangers was stimulated in the last decade by the quest for economic water desalination units. Of particular interest are the multiphase exchangers in the direct-contact freezing processes (*1* to *4*). Also of practical importance are the three-phase direct-contact exchangers where latent heat is transferred from the dispersed volatile fluid to a continuous nonvolatile, immiscible liquid (*5* to *8*). The obvious advantages of utilizing these multiphase exchangers are summarized elsewhere (*9, 10*), and attempts to ellucidate the transfer characteristics and the mechanism of heat transfer in such systems have been reported recently (*9* to *11, 13*).

The relationships between drop diameter and the heat transfer coefficient in direct-contact heat transfer systems without change of phase were reviewed recently (*12*). It was noted that, except at the transition zone between large (2 to 7 mm.) and small (below 1 to 3 mm.) drops, the heat transfer coefficient does not change appreciably with diameter of the drop. Nevertheless, a decrease of the transfer coefficient with increase in drop diameter was noted in a number of experiments, which is in accord with the classical theoretical derivations which predict the transfer coefficient to be inversely proportional to $d^{0.5}$.

Studies of single drops (*9*) and bubbles (*11*) evaporating and condensing, respectively, in stagnant, constant temperature, immiscible liquid media indicated a marked effect of the initial liquid drop diameter on the heat transfer coefficients. However, more information was needed before a quantitative relationship between these parameters could be attempted, and additional single-drop data

Samuel Sideman is at Oklahoma State University, Stillwater, Oklahoma, and Gideon Hirsch is at the Israel Atomic Energy Commission, Dimona, Israel.